Imaging and Tracking of Single GFP Molecules in Solution

Ulrich Kubitscheck, Oliver Kückmann, Thorsten Kues, and Reiner Peters
Institut für Medizinische Physik und Biophysik, Westfälische Wilhelms-Universität, Robert-Koch-Strasse 31, D-48149 Münster, Germany

ABSTRACT Visualization and tracking of single fluorescent molecules is a recent development in optical microscopy holding great promise for the study of cell biological processes. However, all experimental strategies realized so far confined the observation to extremely thin interfacial layers. The detection and characterization of single molecules in three-dimensionally extended systems such as living cells has yet to be accomplished. We show, here, for the first time that single protein molecules can be visualized and tracked in three-dimensional (3D) samples at room temperature. Using a wide-field fluorescence microscope equipped with an Ar^+-laser and a low-light-level CCD camera, single molecules of the green fluorescent protein (GFP) were detected in gels and viscous solutions at depths of up to $\sim$10 μm from the interface. A time resolution of 5 ms was achieved by a high-speed framing mode. The two-dimensional localization accuracy was determined to be $\sim$30 nm. The number of photons emitted by single GFP molecules before photodestruction was found to be $\leq 4 * 10^5$. Freely diffusing GFP molecules could be tracked over up to nine images acquired at a frame rate of $\sim$80 Hz. From the trajectories, the diffusion coefficients of single GFP molecules were derived and found to agree well with expectation and microphotolysis measurements. Our results imply that the visualization and tracking of single molecules in living cells is possible.

INTRODUCTION

The visualization, localization, and spectroscopic characterization of single molecules and single supramolecular complexes by optical techniques has seen remarkable progress in recent years (Xie and Trautman, 1998; Weiss, 1999; Gimzewski and Joachim, 1999). In conventional measurements of large molecular ensembles, only averaged quantities can be determined, single-molecule spectroscopy, however, allows the determination of the distribution of physicochemical quantities. Furthermore, inhomogeneities can be detected in heterogeneous systems, and time-dependent processes studied without synchronization of molecule ensembles.

Several experimental techniques have been developed for the optical detection, imaging, and spectroscopy of single molecules (for reviews see Nie and Zare, 1997; Harada et al., 1998; Moerner and Orrit, 1999) for both room and low temperatures (for review see Basché et al., 1997). The major prerequisite for any optical detection of single fluorophores is the reduction of background signals, which mainly arise from autofluorescence, out-of-focus fluorescence and impurity fluorescence. So far, this has been achieved by reducing the effective depth of the probed volume by total internal reflection, near-field illumination, multiphoton or confocal imaging. Alternatively, two-dimensional (2D) systems, such as glass interfaces and lipid bilayers, have been studied (Sase et al., 1995; Schmidt et al., 1995; Vale et al., 1996; Xu and Yeung, 1997).

In the field of cell biology, a number of single molecule studies dealt with the mobility of receptors in membranes. Using either low-light-level fluorescence or differential interference microscopy, the trajectories of single receptors could be recorded (reviewed by Saxton and Jacobson, 1997; see also Smith et al., 1999 and cited references) and various modes of mobility detected, i.e., directed motion, anomalous or free diffusion. A few single-molecule studies also dealt with structural aspects of the cell nucleus (Kubitscheck et al., 1996; Femino et al., 1998) using fixed cells and using labels carrying several fluorophores. However, the analysis of dynamic processes in vivo requires identification and tracking of single molecules in three-dimensionally extended systems with axial extensions of $\sim$10 μm, which is 1–2 orders of magnitude above what had been achieved so far.

Among the fluorophores that may be relevant for the study of biological systems, the green fluorescent proteins (GFP) assumes an outstanding role (reviewed by Tsien, 1998) because its highly fluorescent chromophore is formed in vivo. GFP has been fused genetically to many cellular proteins thus permitting visualization of the expression and intracellular localization of the constructs in vivo. Furthermore, the mutation of the amino acid sequence of wild-type GFP has resulted in new fluorescent proteins like blue, cyan, or yellow-green GFP. The photophysics of the large Stokes shift of GFP was extensively investigated by ultrafast dynamic studies leading to a detailed understanding of the relationship between protein structure and spectroscopic function. As shown by single-molecule imaging using confocal and total internal reflection microscopy, GFP shows a characteristic blinking behavior (Dickson et al., 1997; Jung et al., 1998). Some GFP mutants were shown to exhibit

Received for publication 23 August 1999 and in final form 30 December 1999.

Address reprint requests to Dr. Ulrich Kubitscheck, Institut für Medizinische Physik und Biophysik, Robert-Koch-Strasse 31, D-48149 Münster, Germany. Tel.: +49-251-835-6932; Fax: +49-251-835-5121; E-mail: kubitsc@uni-muenster.de.

0006-3495/00/04/2170/10 $2.00

long-lived dark states, which can be switched back to on-states by ultraviolet illumination (Dickson et al., 1997). Using the total internal reflection method, Dickson et al., (1996) studied the restricted 3D diffusion of single GFP molecules confined in a polyacrylamide gel matrix.

The present study shows that it is possible to visualize and track single GFP molecules of the mutant S65G/S72A/T203F in 3D systems that extend axially up to 100 μm. Experimental conditions concerning the microscopic setup, the sample preparation, and the fluorescence excitation were optimized. Parameters, such as the total number of photons emitted by single GFP molecules before photodestruction and their localization accuracy, were determined. Single GFP molecules were tracked in viscous solutions, and their diffusion coefficients determined. Thus, the study provides a basis for the application of single molecule visualization to living cells.

MATERIALS AND METHODS

GFP expression and purification

The plasmid pRSET-B encoding the GFP mutant S65G/S72A/T203F (Dickson et al., 1997) was kindly supplied by R. Tsien (San Diego, CA, USA). Expression of GFP in *E. Coli* strain BL21 (DE3) was induced by incubation with isopropyl-β-D-thiogalactosidase (0.5 mM) at 25°C. Purification of the proteins was accomplished by Nickel affinity chromatography according to the manufacturer's protocol (Qiagen, Hilden, Germany). GFP concentration in the stock solution was determined by absorption measurements at 512 nm using the molar extinction coefficient of wildtype GFP (65500 M^{-1} cm^{-1}), which was validated using a BioRad Bradford assay.

Sample preparation

GFP was immobilized in polyacrylamide (PAA) gels by mixing 6 μl of a diluted solution of GFP in phosphate buffered saline (PBS), pH 7.4, with 200 μl of acrylamide (40% wt/wt total concentration of the monomer, 5% wt/wt concentration of the cross-linker), 3 μl of ammonium persulphate (10% wt/vol), and 1 μl of *N,N,N′,N′*-tetramethylethylendiamide. Three microliters of this solution were deposited on a glass slide and covered with a coverslip, resulting in samples with a thickness of ~5 μm. The reaction mixture polymerized within seconds, thereby fixing the GFP molecules. The final concentration of GFP in the gel was adjusted to 5 nM. The refractive index of the gel was determined to be 1.39. All glass surfaces were extensively cleaned before use by sonification in bidistilled water containing 1% Hellmanex II (Hellma, Müllheim, Germany) for 20 min, followed by repetitive rinsing and sonification with bidistilled water. Additional immobile samples were prepared using green fluorescent microbeads of 106-nm diameter (Polysciences, Eppelheim, Germany) as immobile probes instead of single GFP.

GFP was diluted to a final concentration of 20 nM in an 80% and 90% mixture of glycerol in bidistilled water. In additional experiments, Alexa-488 labeled IgG (Molecular Probes, Eugene, OR, USA) was diluted to 2 nM in a 60% mixture of glycerol in phosphate buffered saline. This solution, 5 μl, was filled into a small chamber created by placing a punctured tape spacer between a glass slide and a coverslip. Experiments on these samples were performed at a temperature of 25 ± 2°C. To calculate the theoretical diffusion constant of GFP in these samples according to the Stokes–Einstein equation, $D = kT/f$, where k is the Boltzmann constant, T is absolute temperature, and f is the viscous drag coefficient, we approximated the barrel shape of GFP with a height $2b = 4$ nm and a diameter of $2a = 3$ nm by an elongated ellipsoid of revolution (Ormö et al., 1996; Yang et al., 1996). The shape of the IgG was approximated by an ellipsoid with a height of 15 nm and a diameter of 8 nm. For an ellipsoid, f is given by $6\pi\eta a/\ln(2a/b)$ where η is solvent viscosity (Berg, 1983). Furthermore, using values of 164 and 47 cPoise for η, as extrapolated from the data of Hogman et al. (1961), the theoretical diffusion coefficients for GFP amounted to 2.4 ± 0.6 $\mu m^2/s$ and 0.7 ± 0.2 $\mu m^2/s$ for the 80% and 90% glycerol–water mixtures, respectively. For the Alexa-488 labeled IgG, a value of $D = 4.2 \pm 0.6$ $\mu m^2/s$ is yielded in a solution of 60% glycerol corresponding to a viscosity of 10 cPoise.

Microscopic setup

Single GFP molecules immersed in a thick specimen were observed by means of a wide-field epifluorescence setup using an Axiovert 100 TV (Zeiss, Jena, Germany). Illumination of the sample was performed by 488-nm light from an Ar^+-laser (model 2025, Spectra Physics, Darmstadt, Germany), which passed through a λ/4-plate, and overilluminated the (nearly closed) field iris diaphragm. The field iris diaphragm was then imaged onto the sample by the microscope optics composed of the tube lens and a planapochromatic objective lens (63×, NA 1.4, Zeiss). The image of the diaphragm in the sample had a diameter of ~15 μm over which the illumination intensity was approximately constant. The irradiance in the sample plane was usually adjusted to ~8 kW/cm^2. GFP fluorescence emission was separated from the excitation light by a dedicated GFP filter set (dichromatic beam splitter 505DRLP, emission filter 535RDF45; Omega Optical, Brattleboro VT, USA) and was detected with a cooled slow-scan CCD camera (Quantix, Photometrics, München, Germany) using a CCD chip with 1317 × 1035 pixels (Kodak KAF 1400 Grade 1, Rochester NY, USA) with a pixel size of 6.8 × 6.8 μm^2. The overall light-detection efficiency was determined to be ~3% (see below). The use of a special low autofluorescence immersion oil (Immersol 518 F, Zeiss), which was recently developed specifically for fluorescence microscopy, together with the use of the dedicated GFP filter set, reduced the background fluorescence and the corresponding noise by about 30% in comparison to the situation when the normal green filter cube and a common immersion oil was used. Image acquisition was programmed and performed by means of a Macintosh computer using the IPLab software (Scanalytics Inc., Fairfax, VA, USA). Image integration time was 5–20 ms, the illumination light was switched on only during data acquisition by means of an acousto-optical modulator (Model 304, Coherent, Santa Clara, CA, USA). A user written analysis program was used to determine the position of each fluorescence spot by fitting a 2D Gaussian function to the fluorescence intensity profile using a nonlinear χ^2-minimization routine (Press et al., 1992).

Images were acquired either in the normal slow-scan mode or in the high-speed framing (HSF) mode (Schmidt et al., 1995). Image repetition rate in the slow-scan mode was 4 Hz for a 190 × 120 pixel image. In the HSF mode, the major part of the CCD chip was masked immediately in front of the CCD cover glass such that only a small portion (70 lines) of the total chip area was used for image acquisition. In addition, there was a shadow region of 50 lines neighboring the imaging region resulting from the axial distance between mask and detector surface. After illumination, the excitation light was switched off by means of the AOM (rise time 100 ns), and the contents of the illuminated lines on the chip were shifted into the masked region, which thus served as an intermediate image storage site. This process could be performed rapidly with a minimal shift time of 8 ms (for the total of 120 lines). Because the chip had 1035 lines, this process could be repeated nine times, resulting in a burst of images acquired at an image-acquisition rate of up to 77 Hz at 5-ms integration time.

Mobility measurements by scanning microphotolysis

Diffusion measurements using scanning microphotolysis were performed by means of a confocal laser scanning microscope (Leica TCS, Leica Lasertechnik, Heidelberg, Germany) as described in detail by Kubitscheck et al. (1994). Scanning microphotolysis is a combination of confocal laser scanning microscopy and fluorescence microphotolysis. A confocal laser scanning microscope is equipped with an optical switch able to modulate the power of the laser beam in less than a microsecond while a dedicated computer program precisely coordinates the scanning process and laser beam modulation. Thereby, it is possible to vary the power of the laser beam by a factor of >2000 during scanning at the precision of one resolution element. Here, circular areas were bleached into thin samples of solutions containing GFP with viscosities of 47 and 164 cPoise, and their time development was observed at low, nonbleaching laser powers. The intensity in the photobleached area was averaged, plotted against time, and evaluated for D and the fraction of mobile molecules using the theoretical methods of Axelrod et al. (1976) and Soumpasis (1983).

Localization accuracy

Subresolution objects located in a three-dimensionally extended specimen were observed with specific instrument parameters for the detector pixel size, read-out rate, photon conversion factor, and laser power. All these influence the signal-to-noise ratio (SNR) of the image. The image of a point object or single molecule has a complex 2D intensity profile in the image plane referred to as point spread function (PSF). The PSF determines the spatial resolution that can be achieved by the microscope used and is therefore a limiting parameter in single-molecule localization. The PSF may be calculated on a theoretical basis (Born and Wolf, 1980; Hell et al., 1993). However, because the PSF depends on many parameters, an experimental determination of the PSF is often more meaningful. It can be measured by imaging a fluorescent subresolution object, for example a small fluorescent microbead. If an area detector is positioned in the image plane, the PSF can be well approximated by a 2D Gaussian of the form,

$$f(x, y) = A \exp\left[- \frac{(x - x_c)^2 + (y - y_c)^2}{2\sigma_{xy}^2} \right]. \qquad (1)$$

Here x_c and y_c designate the center coordinates of the Gaussian, marking the position of the observed object, A designates the amplitude, and σ_{xy}^2 designates the radial variance of the 2D Gaussian used to approximate the PSF. The limit at which two particles can be recognized as separate entities is roughly equal to the full width at half maximum (FWHM) of the PSF. This FWHM value is solely determined by the numerical aperture of the objective lens used and the wavelengths of excitation and emitted fluorescence light.

By performing a fit according to Eq. 1 to an observed 2D intensity profile of a subresolution object, all parameters—x_c, y_c, σ_{xy}^2, and a background intensity I_{bg}—may be determined. However, because image acquisition is a stochastic process due to the inherent Poisson noise of light emission, the object center (x_c, y_c) that is found by the χ^2-minimization algorithm is only an estimator for the true object center. We define, as particle localization accuracy, that distance from the found object center, in which the true object center is located with a probability of 0.68, corresponding to a common standard deviation. Usually, the localization accuracy that can be achieved out of images from subresolution objects is at least ten times smaller than the FWHM of the observed intensity distribution. Clearly, the achievable localization accuracy depends strongly on the respective SNR, which we define as

$$\mathrm{SNR} = \frac{I_0}{\sqrt{\sigma_{bg}^2 + \sigma_{I_0}^2}}, \qquad (2)$$

where I_0 designates the maximum signal intensity above background, σ_{bg}^2 the variance of the background intensity values, and $\sigma_{I_0}^2$ the true variance of the maximum signal intensity above the background. $\sigma_{I_0}^2$ must be determined experimentally as described at the end of this paragraph. As mentioned above, all these parameters are dependent on the image-acquisition parameters such as excitation light intensity, signal amplification, and integration time.

Assuming that the χ^2-minimization algorithm locates the object center at the origin (which means no loss of generality), the following expression for the localization accuracy in the image plane can be deduced (Bobroff, 1986; Kues, 1997; Kubitscheck et al., 1999):

$$\Delta x = \sqrt{3.53 \left[\sum_{i=-N}^{N} \sum_{j=-M}^{M} \frac{(I_0^2 x_i^2/\sigma_{xy}^4) \exp[- (x_i^2 + y_j^2)/2\sigma_{xy}^2]}{\sigma_{bg}^2 + \sigma^2(I(x_i, y_j))} \right]^{-1}}. \qquad (3)$$

Here x_i and y_j designate the two discretized spatial coordinates, whereas $2N + 1$ and $2M + 1$ designate the number of pixels in the respective spatial direction used for the localization. The absolute pixel size enters this expression in an indirect way: in the ratio between the radial variances and the discretization intervals $x_{i+1} - x_i$ and $y_{j+1} - y_j$. $\sigma^2(I(x_i, y_j))$ designates the local variance of the signal intensity above background, which is dependent on the local signal intensity. In general, the photon detector and its circuitry introduce an arbitrary amplification factor, making it obligatory to measure the variance as a function of signal intensity for the chosen detector parameters. This can be done by repetitively imaging an object with intensity values covering the complete dynamic range. From this image series, the variance can be determined as a function of the respective average image intensities above background. We can use Eq. 3 to calculate an expectation value for the localization accuracy, Δx, as a function of a maximum signal intensity. Using the definition of the SNR in Eq. 2, we can finally plot the thus determined Δx as a function of the more general SNR.

RESULTS

Visualization of single immobilized GFP molecules

Gels containing low concentrations of GFP were imaged using the epi-fluorescence microscope described above. Without restricting either the excitation light or the sample molecules to a single plane, it was readily possible to acquire images of single GFP molecules in the three-dimensionally extended sample. Figure 1 shows images of a sample with the objective lens focused to the cover glass–gel interface, and to a plane ~2 and 5 μm inside the gel, respectively. The images show several clear and discernible fluorescence maxima. The lateral FWHM of the fluorescence spots in images acquired from the cover glass–gel interface was determined as FWHM = 290 ± 60 nm, (n = 61). Therefore, the fluorescence spots represent diffraction-limited 2D profiles, as would be expected for single GFP molecules.

Focusing deeper into the specimen resulted in images showing darker and larger fluorescence spots (Fig. 1, *B* and *C*). The effect that the amplitude is reduced and the width is increased is probably due to a refractive index (RI) mis-

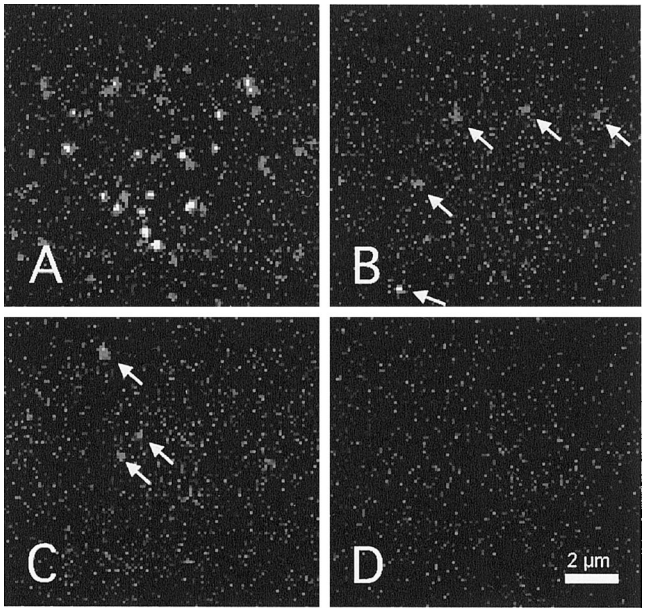

FIGURE 1 Images of single immobile GFP molecules located in different distances to the cover glass–sample interface (A) 0 μm, (*B*) 2 μm, (*C*) 5 μm, (*D*) blank sample at the cover glass–sample interface; *bar*, 2 μm. Excitation power, 7.2 kW/cm^{-2}, image integration time, 20 ms. Apparently, GFP molecules tend to attach to the glass surface before final immobilization. The images show several fluorescence maxima even several micrometers deep in the sample (*arrows*). The decreased image quality deeper in the sample is probably due to the refractive index mismatch between the immersion medium and the specimen.

match between the immersion medium (RI = 1.518) and the specimen (RI = 1.39).

Imaging of blank PAA gels, using PBS instead of protein solution, showed no fluorescence signals (Fig. 1 *D*), thus confirming that the images shown Fig. 1, *A–C* show specific GFP fluorescence. The dark signal of the detector amounted to an offset value of 98.5 ± 1.7 counts (mean count number ± SD). The background signal amounted to 105.0 ± 1.9 counts in samples comprising 5 nM of GFP. Therefore, the fluorescent background was raised by 6.5 counts with an insignificant increase (0.2) in its standard deviation in samples containing GFP. The mean maximum signal amplitude above background, as determined by a fit of single GFP molecules according to Eq. 1, was determined as 8 ± 3 (mean ± SD, n = 61 molecules) at an illumination-light intensity of 8 kW cm^{-2} and an integration time of 10 ms. Therefore, the fluorescence spots could be imaged under these conditions with an SNR of 4.

The evidence that the observed objects are, indeed, single GFP molecules is based on several arguments, which are, however, indirect arguments, as usual in single-molecule microscopy. We already noted that blank probes give absolutely no signals, whereas samples containing GFP show distinct diffraction-limited intensity maxima.

Next, we checked whether the number of the detected spots was proportional to the expected number of molecules. For this analysis, the number of GFP molecules in the PAA gel was adjusted by corresponding dilution of a stock solution. The concentration of the stock solution itself was determined by absorption measurements as described in Materials and Methods. By counting the single-molecule signals in the focal plane 2–4 μm deep in the gel, it was possible to compare the observed number and the expected number of molecules. Assuming an axial extension of the point-spread function of 1 μm, we found a linear relationship between the observed and the expected number of molecules. However, for GFP concentrations between 1 and 26 nM in the gel, we observed generally only about 5% of the expected molecules. This deviation was probably due to several reasons. We found a strong tendency of the molecules to attach to the cover glass even in immobile gels, which presumably occurs before and during the gel polymerization (see Fig. 1). This would reduce the number of observed molecules inside the gel itself. It is possible that a number of GFP molecules in a given preparation still absorbs blue light, but is not fluorescent because of prior photobleaching or incomplete folding of the fluorophore after bacterial expression. Furthermore, we suspect that the reagents added to the gel to induce the polymerization affect the functional integrity of a folded protein, resulting in a loss of fluorescent GFP molecules.

A well-known feature of single GFP molecules is their "blinking" (Dickson et al., 1997). Its observation can be interpreted as an indirect proof for the observation of single molecules. In our experiments, we often observed that the diffraction-limited fluorescence spots vanished and reappeared in a stochastic manner. A high level of fluorescence emission was often interrupted by darker, or completely dark, states. An example is shown in Fig. 2, where, in the upper panel, a time series of images is shown, and, in the lower panel, the corresponding mean fluorescence signal above background.

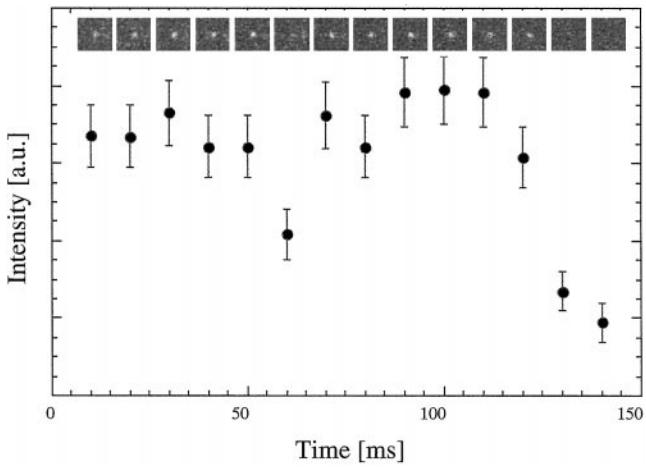

FIGURE 2 Blinking and bleaching of a single GFP molecule. The upper panel shows a time series of images, the graphics give the corresponding mean fluorescence signal above background.

A further indication that the observed fluorescent spots indeed represent single molecules was the observation that all examined time-dependent signals returned to the background signal in an all-or-none manner (Fig. 2). Bleaching of the observed fluorescent spots was instantaneous or "digital." This type of bleaching kinetics is only observed in single-molecule studies. Larger numbers of fluorescent molecules or clusters bleach with an exponential kinetics.

Optimization of the excitation intensity

To determine the optimal excitation light intensity for single-molecule observation, we measured the mean fluorescence intensity emitted by single GFP molecules within 10 ms as a function of the irradiance. The result of these measurements is shown in Fig. 3. The detected fluorescence F approaches a limiting value k_∞, that can be determined as $k_\infty = 11 \pm 4$ counts/ms by a fit of the data to the equation (Schmidt et al., 1995),

$$F = \frac{k_\infty t_{ill}}{1 + (I_s/I_L)}. \quad (4)$$

Here t_{ill} denotes the illumination time, I_L stands for the irradiance, and I_S designates the saturation irradiance, which, in our case, was determined as 11 ± 1.5 kW/cm^2. At this irradiance, half of the maximum fluorescence is emitted. To achieve longer observation times, we chose an irradiance slightly below that value, namely ~8 kW/cm^2, because we wanted to avoid fluorescence saturation of the GFP. Higher irradiances will only lead to an increase in fluorescence background, whereas the specific GFP fluorescence will remain constant.

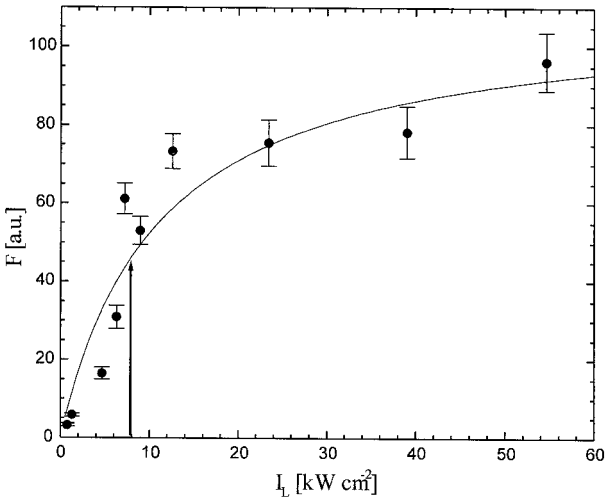

FIGURE 3 Fluorescence saturation of single GFP molecules as a function of the irradiance. Mean fluorescence intensity emitted by single GFP molecules within 10 ms was measured as a function of the incident irradiance (*symbols*). The data were fitted to Eq. 4 (*full line*), resulting in a value of 11 ± 4 kW/cm^2, at which 50% of the maximum fluorescence is emitted. *Arrow*, experimental irradiance.

Determination of the maximum illumination time before photobleaching

The usefulness of a fluorescent probe is predominantly determined by its photostability. Therefore, we measured the total number of photons emitted by single GFPs during the lifetime until photodestruction. To this end, we had to determine the detection efficiency of our system, η_{total}, which is given by

$$\eta_{total} = \eta_{NA} * T_{obj} * T_{bs} * T_{TL} * T_{cw} * Q_{CCD}$$
$$= 0.30 * 0.85 * 0.40 * 0.90 * 0.95 * 0.33.$$

Here, η_{NA} designates the collection efficiency of the objective lens due to the limited opening angle, T_{obj} the transmittance of the objective lens, T_{bs} the transmittance of the dichromatic beam splitter and the emission band-pass filter, T_{TL} designates the transmittance of the tube lens, T_{cw} the transmittance of the camera window, and Q_{CCD} the detection quantum efficiency of the CCD sensor. Altogether, we found that $\eta_{total} = 0.028 \pm 0.005$. Using the photoelectron-to-digital unit-conversion factor κ of the CCD in the collection mode used ($\kappa = 10$), we found that the number of total detected counts, N_{count}, could be related to the total number of emitted photons, N_p, according to $N_p = 357 \cdot N_{count}$.

We acquired multiple-image series of single GFP until they appeared totally photobleached. Then, the integrated number of detected counts above background for single GFP was determined and translated into a respective total number of emitted photons. In Fig. 4 *A*, the frequency distribution of these values is given for a total of 93 single GFP molecules. From these data, it can be deduced that, on the average, GFPs emit $110{,}000 \pm 60{,}000$ photons during their lifetime. A small number of 9% emits ≥200,000 up to a maximum of 400,000 photons. Figure 4 *B* shows the number of photons emitted by single GFP in 10-ms time intervals at our standard excitation intensity of 8 kW/cm^2. This histogram displays the distribution of emitted photon per 10 ms in comparison to the distribution of the background photons. On the average, the GFP emit $21{,}000 \pm 8000$ photons in 10 ms while excited with 8 kW/cm^2. That means that they can be observed for a time period of 10–100 ms under the irradiance conditions used.

Localization accuracy

Application of the procedure described in Materials and Methods for estimating the GFP localization accuracy resulted in the following. For an integration time of 10 ms and 1 MHz readout rate of the CCD, we found $\sigma^2(I) = 0.106$ I. The CCD pixel size amounted to 108 nm in object space due

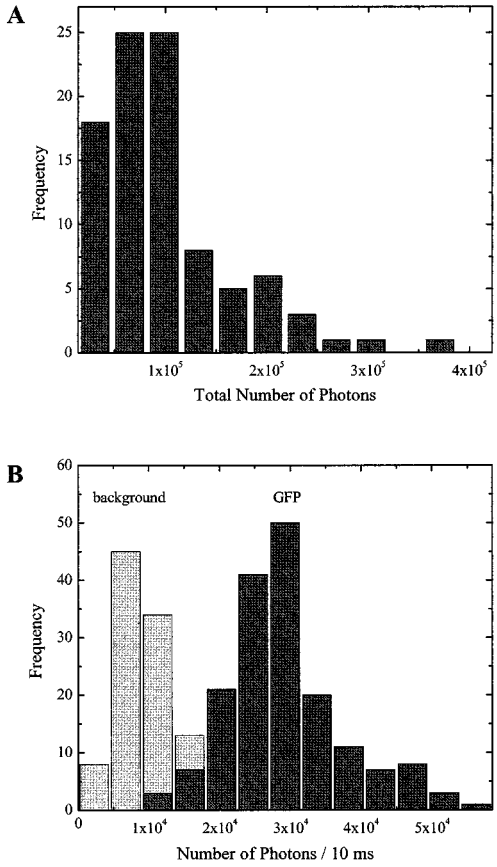

FIGURE 4 Light emission of single GFP molecules. (*A*) Frequency distribution of the total number of photons emitted by single GFP molecules ($N = 93$). (*B*) Frequency distribution of the number of photons emitted by single GFP within 10-ms time intervals at an excitation intensity of 8 kW/cm^2 in comparison to the distribution of the background photons. Multiple images of single GFP molecules were acquired until they were photobleached. The integrated number of detected counts above background for single GFP was determined and translated into the number of emitted photons, assuming a detection efficiency of 2.8% and using a photoelectron-to-digital unit conversion factor of 10.

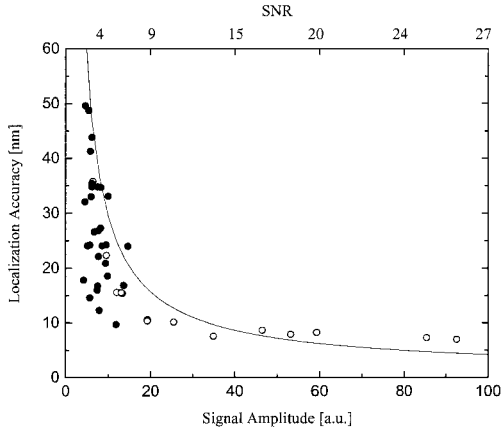

FIGURE 5 Localization accuracy as a function of the signal amplitude and the SNR. Theoretical calculation according to Eqs. 2 and 3 (*full line*, see text), and data obtained by repetitive imaging of nanobeads (*open symbols*) and single GFP molecules (*closed symbols*). Immobile fluorescent subresolution microbeads (diameter 106 nm) and single GFP molecules were repetitively imaged. In the resulting image series, the center positions of the fluorescence maxima were determined by χ^2-fits using 2D Gaussians, and the standard deviations of the resulting center positions were calculated (Kubitscheck et al., 1999). These values correspond to the localization accuracies, and they were plotted as functions of the maximum signal amplitude and the SNR.

to the use of the 63× objective lens. The standard deviation of the 2D Gaussian approximating the PSF was determined by imaging subresolution fluorescence beads, and resulted in $\sigma_{xy} = 122$ nm, corresponding to an FWHM of 287 nm. The standard deviation of the background signal intensity corresponded to $\sigma_{bg} = 1.9$. Using these parameters, the theoretical 2D localization accuracy was calculated using Eqs. 2 and 3 as a function of the SNR. The result is shown in Fig. 5 by the full line for this standard set of experimental parameters. For a mean maximum amplitude of 8, as determined above, the SNR of single GFP corresponded to ~4. The theoretical localization accuracy for this SNR can be determined as <37 nm. At a SNR of 10, the theoretical localization accuracy would amount to ±14 nm.

To validate the theoretical estimation for the localization accuracy attainable with a 2D Gaussian function fitted to the diffraction-limited image of submicroscopic objects, an experimental determination of the localization accuracy was performed. To this end, a specimen composed of immobile fluorescent subresolution microbeads with a diameter of 106 nm was repetitively imaged. In the resulting image series, the center positions of the objects were determined by χ^2-fits of 2D Gaussians to the diffraction-limited image of the beads, and the standard deviations of the center positions were calculated (Kubitscheck et al., 1999). These values, representing the localization accuracy, were plotted as a function of the maximum signal amplitude or the SNR (*open symbols* in Fig. 5). We found that the localization accuracies approached ±7 nm. As the data in Fig. 5 show, the localization accuracy for low SNRs was experimentally better than theoretically expected. This systematic deviation is presumably due to the fact that the theoretical localization accuracy was derived under the assumption that the measured signal follows a Gaussian statistic, whereas, in reality, it follows a Poisson statistic. Only for larger signal intensities a Gaussian distribution well approximates the Poisson distribution. Nevertheless, the theoretical estimation provides a quick estimate for the upper limit for the achievable localization accuracy.

Repetitive imaging of single immobilized GFP molecules allowed experimental determination of their localization accuracy. The results are shown by the closed symbols in Fig. 5. The averaged amplitude I_0 of all GFPs from several image series was $I_0 = 8$, resulting in a mean SNR of ~4. Therefore, on the average, single GFP can be localized with an accuracy of 27 nm under the chosen imaging conditions.

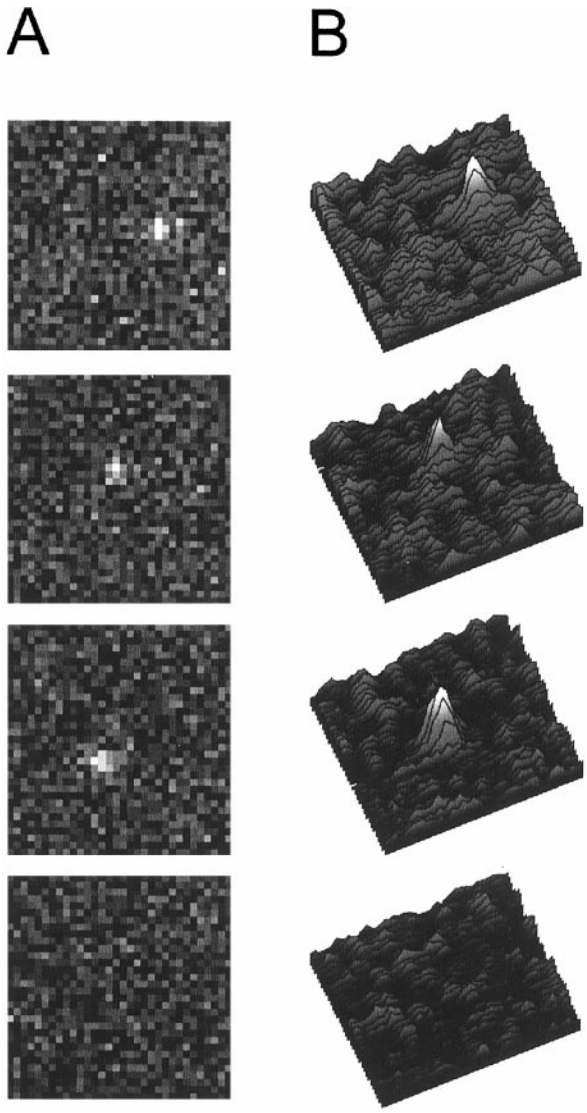

FIGURE 6 Diffusion of a GFP molecule in 80% glycerol. (*A*) Time series of raw images. (*B*) Surface plots of smoothed and background subtracted raw images. The field size shown is $3.6 \times 3.6\ \mu m^2$. Images were acquired in the high-speed framing mode with an integration time of 5 ms per image and an image lag time of 16 ms. Presumably, the molecule bleached during acquisition of the third image.

Tracking of single GFP and IgG molecules

The above results imply that it should be possible to observe single GFP molecules in solution, and to follow their trajectories as long as they reside in the focal plane of the objective lens. We would then extract a set of space–time coordinates, $\{x(t_i), y(t_i), t_i\}$, which represents a 2D projection of their 3D trajectory. Here, t_i designates the discrete observation time points. If the molecules are moving by free diffusion in solution, their average 2D mean square displacement $\langle \Delta x^2 + \Delta y^2 \rangle$ is related to the diffusion coefficient, D, by

$$\langle \Delta x^2 + \Delta y^2 \rangle = 4Dt.$$

Figure 6 *A* shows a representative image sequence, where a single GFP molecule in an 80% glycerol/water mixture is tracked over three images that were acquired in the HSF mode with an integration time per image of 5 ms and an image lag time of 16 ms at a temperature of 25°C (see Table I). In Fig. 6 *B*, a surface plot representation of the data after background subtraction and application of a single 3×3 mean filter is shown. This representation stresses the high SNR of the trajectory measurement. Most probably, the molecule bleached during acquisition of the third image. For viscosities of 164 cPoise (90% glycerol/buffer mixture) and 47 cPoise (80% glycerol/buffer mixture), we evaluated 120 and 90 single molecule trajectories, respectively, and plotted the average mean square displacements (MSD) against time (Fig. 7). The error bars in Fig. 7 correspond to the SD of the mean values. They may appear surprisingly large, but they indeed correspond well to the theoretically expected standard deviation of the MSD, $4\sqrt{2}Dt$. By fitting a straight line to the data, we determined an average diffusion coefficient of $0.9 \pm 0.1\ \mu m^2/s$ for $\eta = 164$ cPoise, and $3.0 \pm 0.1\ \mu m^2/s$ for $\eta = 47$ cPoise. These values were in good agreement with the theoretical expectation. For comparison, we performed conventional scanning microphotolysis measurements of GFP in respective bulk solutions and measured diffusion coefficients of $0.6 \pm 0.2\ \mu m^2/s$ (mean $\pm$ SD) for $\eta = 164$ cPoise and $2.0 \pm 0.7\ \mu m^2/s$ for

TABLE 1 Diffusion constants *D* of various probes in viscous solution as determined by theory, single particle tracking (SPT), and bulk microphotolysis measurements using the SCAMP method

Probe molecule	Viscosity (cPoise)	Integration time (ms)	Lag time (ms)	D_{SPT}* ($\mu m^2/s$)	D_{Theory}† ($\mu m^2/s$)	D_{SCAMP}‡ ($\mu m^2/s$)
GFP	164	10	32	0.9 ± 0.1	0.7 ± 0.2	0.6 ± 0.2
GFP	47	5	16	3.0 ± 0.1	2.4 ± 0.6	2.0 ± 0.7
IgG	10	2	8	3.6 ± 0.3	4.2 ± 0.6	

*Integration times were 10, 5, and 2 ms and lag times between two subsequent images were 32, 16, and 8 ms for $\eta = 164$, 47, and 10 cPoise, respectively.
†All theoretical diffusion constants were calculated assuming ellipsoid shapes (Berg, 1983) for the molecules (height 4 nm and 15 nm, diameter 3 nm and 8 nm for the GFP and IgG, respectively) for a temperature of 25 ± 0.2°C as present during the measurements. Error estimations are due to uncertainties in temperature of ± 0.2°C, and assuming an error in glycerol concentration of $\pm 1\%$.
‡Values given are mean values $\pm$ standard deviation.

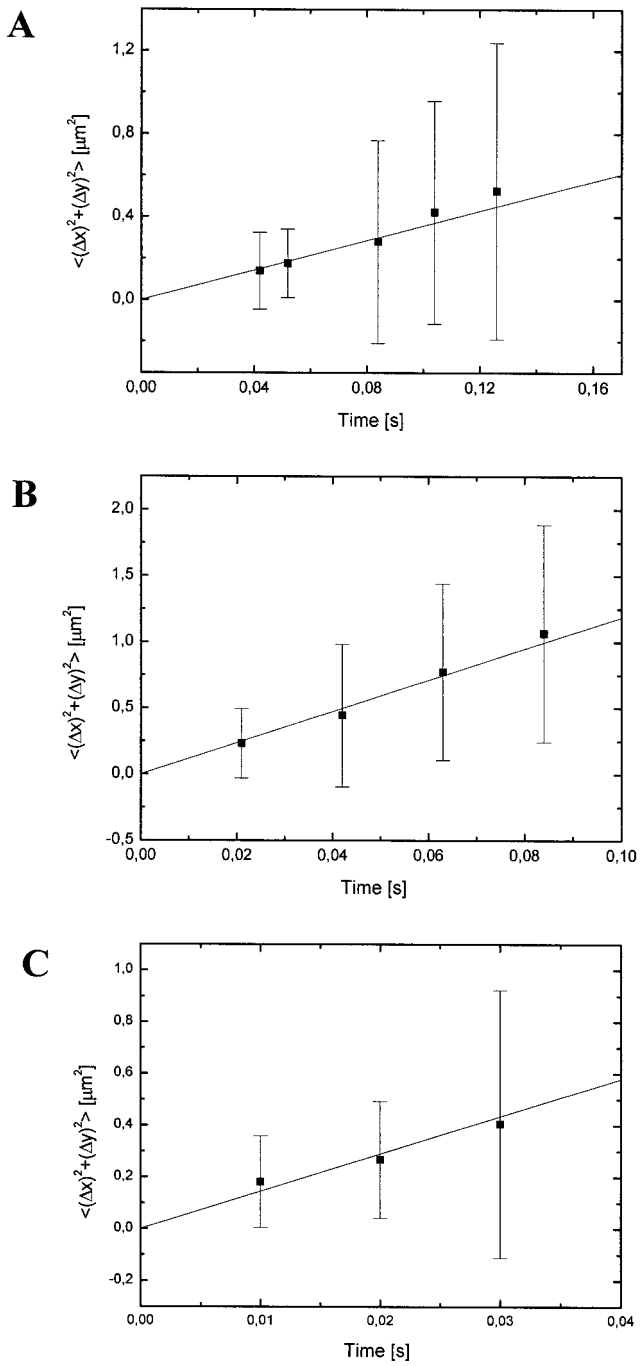

FIGURE 7 Dependence of single molecule mean square displacements as a function of time (mean ± standard deviation). (*A*) GFP molecules ($N = 120$) at a viscosity of 164 cPoise (90% glycerol/buffer mixture). (*B*) GFP molecules ($N = 90$) at a viscosity of 47 cPoise (80% glycerol/buffer mixture). (*C*) Alexa-488 labeled IgG molecules ($N = 38$) at a viscosity of 10 cPoise (60% glycerol/buffer mixture). All measurements were performed at a temperature of 25°C.

$\eta = 47$ cPoise. Data-acquisition parameters, and all results concerning the diffusion measurements are compiled in Table I.

DISCUSSION

The real-time observation of single fluorescent molecules in cellular systems is important for the understanding of dynamic processes on a molecular level in vivo. To achieve this goal, single molecules must be visualized in three-dimensionally extended systems with axial extensions in the size range of single cells. These axial dimensions, however, are an order of magnitude larger than all geometries that have been analyzed so far. Due to the attempt to suppress background signals, single-molecule observations were restricted to ultrathin samples, to events very close to interfaces, or were performed using confocal detection systems. The latter ones are generally too slow to monitor molecular transport inside cell biological systems.

In this contribution, we showed that it is possible to detect, image, and track single GFP molecules that were dispersed inside a sample with axial dimensions as large as 100 μm without the use of any technique restricting the observation volume. We presented images of single molecules that were located in sample depths of up to 5 μm. With decreasing SNR, GFP molecules were detectable in depths of 10–15 μm. These values are in the axial size range of adherent biological cells, and hence, they suggest that it should be feasible to observe single molecules inside living cells.

We attribute the feasibility of single-molecule observation in the 3D spatially extended samples several micrometers away from any interface to a combination of measures taken. Using a field iris diaphragm in the excitation light-path illumination of the object field was limited to an area of 170 μm^2 through a high numerical aperture objective lens. This resulted in an axial confinement of the irradiance near the focal plane, albeit allowing observation of an extended field. Special immersion oil with low autofluorescence, ultrapure solutions, and carefully cleaned coverslips and glass slides were used to lower the autofluorescence background. Dichromatic and band-pass filters optimized for GFP, a detection light path with a minimum number of optical components, and a highly sensitive slow-scan CCD camera were used to maximize the detection efficiency. Furthermore, we adjusted the laser irradiation to optimal fluorescence excitation while carefully avoiding excited state saturation.

GFP represents a key candidate as a protein marker in intact cells and in vitro systems. Therefore, it was chosen as a model molecule to be visualized and tracked. First, immobile GFP molecules (mutant S65G/S72A/T203F) were visualized with an SNR of 4, and located with an average accuracy of 27 nm. Evaluation of about 100 single immobile GFP molecules showed that they emit 110,000 ± 60,000 photons during their lifetime, whereas about 10% emit more than 200,000, up to a maximum of 400,000 photons, before photodestruction. Mobile single GFP molecules were observed in glycerol–water mixtures with viscosities of 47 and

164 cPoise. Observed with an image-integration time of 5–10 ms, the diffusion coefficients of GFP molecules were determined by SPT by analyzing their averaged mean square displacement as a function of time. In this manner, diffusion coefficients of $D_{47\text{cPoise}} = 3.0 \pm 0.1\ \mu\text{m}^2/\text{s}$, and $D_{164\text{cPoise}} = 0.9 \pm 0.1\ \mu\text{m}^2/\text{s}$ were determined. These values agreed well with expectations based on theoretical reasons and mobility measurements on bulk solutions.

With the present setup, we perceive a thin section of the 3D extended specimen. Hence, we observe a 2D projection of the 3D diffusion trajectory. We chose the total HSF image-acquisition time to be smaller than the mean escape time of the molecules out of the observed section. Depending on what molecules or particles are observed, it appears also feasible to observe a larger fraction of the total 3D space by rapidly shifting the sample using a piezo-controlled microscope table. An HSF series of images could then be used to acquire a full 3D image stack of the sample.

The results obtained in this study allow an evaluation of GFP tags for use in single-molecule tracking in living cellular systems. From a total number of ~21,000 emitted photons per 10 ms, ~3% could be detected and allowed a localization with an accuracy below 40 nm at our current background signal. Thereby, single GFP molecules could be detected over up to 10 images before photodestruction. Clearly, a high autofluorescence background signal would reduce the attainable SNR. We found, however, that, for example, in living cell nuclei, the standard deviation of the background fluorescence is increased only by 20% compared to clean buffer solutions, where it is only 5% larger than the standard deviation of the dark current signal of the CCD camera used. This increase is insignificant, and would not hinder single-molecule detection. Inside the cytoplasm, however, autofluorescence is very inhomogeneous and significantly higher with a correspondingly strong increase in background noise, making single-molecule detection more problematic.

We could detect single GFP molecules moving with a diffusion coefficient of up to $D = \sim 3\ \mu\text{m}^2/\text{s}$, corresponding to a mean square displacement of $0.12\ \mu\text{m}^2$ during the 10-ms integration time. This value was approximately equal to the area of the Airy disk of the objective lens we used ($0.18\ \mu\text{m}^2$). Hence, the movement of the molecule during the image integration time did not notably blurr the single-molecule image. An extensive blurring would result in a serious reduction of the SNR, which could render single-molecule observation impossible. These considerations suggest that detection of fast moving molecules is feasible, if probes brighter than single GFP molecules are used, e.g., proteins with several GFP molecule tags. To illustrate this, we imaged and tracked a fluorescently labeled antibody in a solution with a viscosity of 10 cPoise at 25°C (see Fig. 7 *C*). This value corresponds to the average viscosity of the nucleoplasm (Lang et al., 1986; Seksek et al., 1997). Because of the strong fluorescence emission of this protein, which was labeled with 6.8 Alexa-488 fluorophores on the average, image integration times could be reduced to 1–2 ms only. Single antibodies were tracked over several images, and their diffusion coefficient was determined in agreement with the theoretical expectation (see Table 1). Therefore, we suppose that it will soon be possible to observe single-molecule events inside living cells, provided care is taken for an overall low fluorescence background, and signal brightness, integration time, and velocity of the observed probes are appropriately matched.

Support from the Deutsche Forschungsgemeinschaft (DFG grant Ku 975/3–1) is gratefully acknowledged.

We thank Katharina Zerf for expressing and purifying the GFP.

REFERENCES

Axelrod, D., D. E. Koppel, J. Schlessinger, E. Elson, and W. W. Webb. 1976. Mobility measurement by analysis of fluorescence photobleaching recovery kinetics. *Biophys. J.* 16:1055–1069.

Basché, T., W. E. Moerner, M. Orrit, U. P. Wild., editors. 1997. Single-Molecule Optical Detection, Imaging and Spectroscopy. VCH Press, Weinheim, Germany.

Berg, H. C. 1983. Random Walks in Biology. Princeton University Press, Princeton, NJ.

Bobroff, N. 1986. Position measurement with a resolution and noise-limited instrument. *Rev. Sci. Instrum.* 57:1152–1157.

Born, M., and E. Wolf. 1980. Principles of Optics, 6th ed. Cambridge University Press, New York. 435–445.

Dickson, R. M., D. J. Norris, Y.-L. Tzeng, and W. E. Moerner. 1996. Three-dimensional imaging of single molecules solvated in pores of polyacrylamide gels. *Science.* 274:966–969.

Dickson, R. M., A. B. Cubitt, R. Y. Tsien, and W. E. Moerner. 1997. On/off blinking and switching behaviour of single molecules of green fluorescent protein. *Nature.* 388:355–358.

Femino, A. M., F. S. Fay, K. Fogarty, and R. H. Singer. 1998. Visualization of single RNA transcripts in Situ. *Science.* 280:585–590.

Gimzewski, J. K., and C. Joachim. 1999. Nanoscale science of single molecules using local probes. *Science.* 283:1683–1688.

Harada, Y., T. Funatsu, M. Tokunaga, K. Saito, H. Higuchi, Y. Ishii, and T. Yanagida. 1998. Single molecule imaging, and nanomanipulation of biomolecules. *Meth. Cell Biol.* 55:117–129.

Hell, S., G. Reiner, C. Cremer, and E. H. K. Stelzer. 1993. Abberations in confocal fluorescence microscopy induced by mismatches in refractive index. *J. Microsc.* 169:391–405.

Hogman, C. D., R. C. Wheast, R. S. Shankland, and S. M. Selby. 1961. Handbook of Chemistry and Physics. 44th ed. The Chemical Rubber Publishing Co., Cleveland, Ohio.

Jung, G., J. Wiehler, W. Göhde, J. Tittel, T. Basché, B. Steipe, and C. Bräuchle. 1998. Confocal microscopy of single molecules of the green fluorescent protein. *Bioimaging.* 6:54–61.

Kubitscheck U., P. Wedekind, and R. Peters. 1994. Lateral diffusion measurement at high spatial resolution by scanning microphotolysis in a confocal microscope. *Biophys. J.* 67:948–956.

Kubitscheck U., P. Wedekind, O. Zeidler, M. Grote, and R. Peters. 1996. Single nuclear pores visualized by confocal microscopy and image processing. *Biophys. J.* 70:2067–2077.

Kubitscheck, U., T. Kues, and R. Peters. 1999. Visualization of the nuclear pore complex and its localization at nanometer accuracy. *Meth. Enzymol.* 307:207–230.

Kues, T. 1997. Zur Genauigkeit der Lokalisierung immobiler und mobiler submikroskopischer Partikel durch konfokale Laser-Scanning-Mikroskopie und Bildanalyse. Diploma thesis, Westfälische Wilhelms-Universität Münster, Münster, Germany.

Lang, I., M. Scholz, and R. Peters. 1986. Molecular mobility and nucleocytoplasmic flux in hepatoma cells. *J. Cell Biol.* 102:1183–1190.

Moerner, W. E., and M. Orritt. 1999. Illuminating single molecules in condensed matter. *Science.* 283:1670–1676

Nie, S., and R. N. Zare. 1997. Optical detection of single molecules. *Ann. Rev. Biophys. Biomol. Struct.* 26:567–596.

Ormö, M., A. B. Cubitt, K. Kallio, L. A. Gross, R. Tsien, and S. J. Remington. 1996. Crystal structure of the aequorea victoria green fluorescent protein. *Science.* 273:1392–1395.

Press, W., S. A. Teukolsky, W. V. Vetterling, and B. P. Flannery. 1992. Numerical Recipes in C. Cambridge University Press, Cambridge.

Sase, I, H. Miyata, J. E. Corrie, J. S. Craik, and K. Kinosita. 1995. Real time imaging of single fluorophores on moving actin with an epifluorescence microscope. *Biophys J.* 69:323–8.

Saxton, M. J., and K. Jacobson. 1997. Single-particle tracking: applications to membrane dynamics. *Annu. Rev. Biophys. Biomol. Struct.* 26: 373–399.

Schmidt, T., G. J. Schütz, W. Baumgartner, H. J. Gruber, H. Schindler. 1995. Characterization of photophysics and mobility of single molecules in a fluid lipid membrane. *J. Phys. Chem.* 99:17662–17668.

Seksek, O., J. Biwersi, and A. S. Verkman. 1997. Translational diffusion of macromolecule-sized solutes in cytoplasm and nucleus. *J. Cell Biol.* 138:131–142.

Smith, P. R., I. E. G. Morrison, K. M. Wilson, N. Fernández, and R. J. Cherry. 1999. Anomalous diffusion of major histocompatibility complex class I molecules on HeLa cells determined by single particle tracking. *Biophys. J.* 76:3331–3344.

Soumpasis, D. M. 1983. Theoretical analysis of fluorescence photobleaching recovery experiments. *Biophys. J.* 41:95–97.

Tsien, R. Y. 1998. The green fluorescent protein. *Annu. Rev. Biochem.* 67:509–544.

Vale, R. D., T. Funatsu, D. Pierce, L. Romberg, Y. Harada, and T. Yanagida. 1996. Direct observation of single kinesin molecules moving along microtubules. *Nature.* 380:451–453.

Weiss, S. 1999. Fluorescence spectroscopy of single biomolecules. *Science* 283:1676–1683

Xie, X. S., and J. K. Trautman. 1998. Optical studies of single molecules at room temperature. *Ann. Rev. Phys. Chem.* 49:441–480.

Xu, X.-H., and E. S. Yeung. 1997. Direct measurement of single-molecule diffusion and photodecomposition in free solution. *Science.* 275: 1106–1109.

Yang, F., L. G. Moss, G. N. Phillips, Jr. 1996. The molecular structure of green fluorescent protein. *Nature Biotech.* 14:1246–1251.